JOURNAL OF GEOPHYSICAL RESEARCH, VOL. 117, A00M05, doi:10.1029/2012JA017822, 2012

Survey of coherent ~1 Hz waves in Mercury's inner magnetosphere from MESSENGER observations

Scott A. Boardsen,[1,2] James A. Slavin,[3] Brian J. Anderson,[4] Haje Korth,[4] David Schriver,[5] and Sean C. Solomon[6,7]

Received 11 April 2012; revised 5 July 2012; accepted 7 July 2012; published 22 September 2012.

[1] We summarize observations by the MESSENGER spacecraft of highly coherent waves at frequencies between 0.4 and 5 Hz in Mercury's inner magnetosphere. This survey covers the time period from 24 March to 25 September 2011, or 2.1 Mercury years. These waves typically exhibit banded harmonic structure that drifts in frequency as the spacecraft traverses the magnetic equator. The waves are seen at all magnetic local times, but their observed rate of occurrence is much less on the dayside, at least in part the result of MESSENGER's orbit. On the nightside, on average, wave power is maximum near the equator and decreases with increasing magnetic latitude, consistent with an equatorial source. When the spacecraft traverses the plasma sheet during its equatorial crossings, wave power is a factor of 2 larger than for equatorial crossings that do not cross the plasma sheet. The waves are highly transverse at large magnetic latitudes but are more compressional near the equator. However, at the equator the transverse component of these waves increases relative to the compressional component as the degree of polarization decreases. Also, there is a substantial minority of events that are transverse at all magnetic latitudes, including the equator. A few of these latter events could be interpreted as ion cyclotron waves. In general, the waves tend to be strongly linear and characterized by values of the ellipticity <0.3 and wave-normal angles peaked near 90°. Their maxima in wave power at the equator coupled with their narrow-band character suggests that these waves might be generated locally in loss cone plasma characterized by high values of the ratio β of plasma pressure to magnetic pressure. Presumably both electromagnetic ion cyclotron waves and electromagnetic ion Bernstein waves can be generated by ion loss cone distributions. If proton β decreases with increasing magnetic latitude along a field line, then electromagnetic ion Bernstein waves are predicted to transition from compressional to transverse, a pattern consistent with our observations. We hypothesize that these local instabilities can lead to enhanced ion precipitation and directly feed field-line resonances.

Citation: Boardsen, S. A., J. A. Slavin, B. J. Anderson, H. Korth, D. Schriver, and S. C. Solomon (2012), Survey of coherent ~1 Hz waves in Mercury's inner magnetosphere from MESSENGER observations, *J. Geophys. Res.*, *117*, A00M05, doi:10.1029/2012JA017822.

1. Introduction

[2] Highly coherent waves with frequencies near ~1 Hz were observed in Mercury's magnetosphere during the first (M1) [*Boardsen et al.*, 2009a] and second (M2) [*Boardsen et al.*, 2009b] near-equatorial flybys of the MErcury Surface, Space ENvironment, GEochemistry, and Ranging (MESSENGER) spacecraft. They were also briefly (~38 s burst) observed near an equatorial crossing during the first Mariner 10 flyby of Mercury in 1974 [*Russell*, 1989]. During both M1 and M2, narrow-band, ultra-low-frequency (ULF) waves were

[1]Heliophysics Science Division, NASA Goddard Space Flight Center, Greenbelt, Maryland, USA.
[2]Goddard Planetary Heliophysics Institute, University of Maryland, Baltimore, Maryland, USA.
Corresponding author: S. A. Boardsen, Heliophysics Science Division, NASA Goddard Space Flight Center, Greenbelt, MD 20771, USA. (scott.a.boardsen@nasa.gov)
[3]Department of Atmospheric, Oceanic and Space Sciences, University of Michigan, Ann Arbor, Michigan, USA.
[4]Johns Hopkins University Applied Physics Laboratory, Laurel, Maryland, USA.
[5]Institute of Geophysics and Planetary Physics and Department of Physics and Astronomy, University of California, Los Angeles, California, USA.
[6]Department of Terrestrial Magnetism, Carnegie Institution of Washington, Washington, D. C., USA.
[7]Lamont-Doherty Earth Observatory, Columbia University, Palisades, New York, USA.

0148-0227/12/2012JA017822

detected from just after closest approach nearly to the outbound magnetopause crossing. Bursts of waves were recorded almost continuously during M1 and M2 over approximately 9 min intervals on both encounters. During these wave observations MESSENGER covered a range in radial distance from 1.1 to 1.9 R_M (where R_M is Mercury's radius), in magnetic local time (MLT) from 2 to 6 h, and in magnetic latitude from $-23°$ to $-15°$. The wave frequency varied between the He^+ cyclotron frequency f_{cHe+} and the proton cyclotron frequency f_{cH+}. An outbound boundary layer was encountered on both flybys, and wave power was a factor of ~10 greater inside the boundary layer than outside the layer. No frequency drift was observed within the boundary layer, whereas a frequency drift was observed during M1 in the region inward of the boundary layer. The magnetosphere was quiet during M1 and highly disturbed during M2, and the overall wave power was 4 to 5 times larger during M2 than during M1. Near the closest approach (CA) of each flyby trajectory, the power in the wave component oriented parallel to the local magnetic field tended to be larger than the power in the component perpendicular to the field, whereas away from CA the perpendicular power dominated. There was a large scatter in both the ellipticity and wave-normal angle, but the ellipticity values were skewed toward right-handedness, and the wave-normal angles tended to be greater than 45°.

[3] There have been many explanations for these waves. *Russell* [1989] proposed that they are standing Alfvén waves. However, due the substantial field-aligned fluctuations, *Blomberg* [1997] and *Southwood* [1997] argued against an explanation involving purely standing Alfvén waves. Because these waves are primarily seen at frequencies between f_{cHe+} and f_{cH+}, and because a sizable heavy ion component has been documented in Mercury's magnetospheric plasma [*Zurbuchen et al.*, 2008; *Raines et al.*, 2011], the effects of heavy ions must be important in wave generation. *Zurbuchen et al.* [2011] recently reported that heavy ions with values of mass per charge near that of Na^+, termed the Na^+ group, contribute substantially to the total plasma pressure in the near-Mercury nightside plasma sheet.

[4] A number of studies have employed cold-plasma theory to explore the effects of ions on waves in the light-ion frequency range [*Othmer et al.*, 1999; *Glassmeier et al.*, 2003; *Kim and Lee*, 2003; *Klimushkin et al.*, 2006; *Kim et al.*, 2008, 2011]. *Othmer et al.* [1999] and *Klimushkin et al.* [2006] found that crossover frequencies, across which the polarization of a wave mode changes sign, are preferred frequencies for modified field-line resonances. However, *Kim et al.* [2008] showed from simulations that coupling occurs at ion-ion resonance frequencies. *Kim et al.* [2011] showed further that this ion-ion hybrid resonance coupling at Mercury is more efficient than the Alfvén resonance for a plasma composed of H^+ and Na^+, and that the field-aligned resonant frequency structure can be complex and discontinuous and highly dependent on the density ratio of Na^+ to H^+. An ion-ion hybrid frequency is located between each pair of neighboring ion cyclotron frequencies and just above the Bushsbaum-Bers frequency for that ion pair (a discussion of the difference between Buchsbaum-Bers resonances and ion-ion hybrid resonances is given by *Lee et al.* [2008]). If these waves are field-line resonances, their spatial distribution could be used to demarcate boundaries between open and closed field lines.

[5] On the basis of MESSENGER flyby observations, *Boardsen et al.* [2009a, 2009b] suggested that because of their substantial compressional component these oscillations are not field-aligned resonances but rather quasi-trapped waves, similar to fast magnetosonic waves observed at frequencies near f_{cH+} near the equatorial plasmapause of Earth. Moreover, *Boardsen et al.* [2009a, 2009b] predicted that the waves would be confined in latitudinal extent. In Mercury's inner magnetosphere the planetary loss cone half angle varies from 67° at an L-shell of 1.1 to 20° at an L-shell of 2.0 (where the L-shell parameter defines an axisymmetric surface of those lines of magnetic force from the dipole component of Mercury's internal field that intersect the magnetic equator at a distance $L\,R_M$ from the dipole center), leading to strongly non-Maxwellian velocity distributions that are expected to be highly unstable. Such anisotropic plasma distributions, with a temperature in the direction perpendicular to the local magnetic field greater than that in the parallel direction, have been observed in the global hybrid simulations of the flybys [*Trávníček et al.*, 2010]. These instabilities lead in turn to the development of plasma waves that can scatter ions into the loss cone from which they precipitate onto Mercury's surface [*Schriver et al.*, 2011].

[6] That these ULF waves at Mercury are poorly understood is at least in part because of the limited spatial and temporal coverage of the flybys. The insertion of the MESSENGER spacecraft into a near-polar orbit in March 2011 has allowed mapping of these waves against magnetic latitude and magnetic local time. Here we characterize the spectral content, amplitudes, and polarization properties of these waves on the basis of orbital observations.

[7] The variation of the MESSENGER orbit about Mercury as Mercury orbits the Sun is shown in Figure 1. The orbital plane of MESSENGER lies in the dawn-dusk plane when Mercury is near perihelion (0.31 AU) and aphelion (0.47 AU). Near perihelion, MESSENGER's periapsis is on Mercury's dawn side, and near aphelion MESSENGER's apoapsis is on the dusk side. The orbital plane of MESSENGER lies near the noon-midnight plane of Mercury when the planet's heliocentric distance is ~0.37 AU. Near 0.37 AU MESSENGER samples either the near tail (with Mercury traveling outbound from the Sun) or the deep tail (with Mercury traveling toward the Sun) of Mercury's magnetosphere. This information, combined with theory, aids in the physical interpretation of these waves, and thus in determining the role they play in Mercury's magnetosphere. In this paper we present examples, statistics, and our interpretation of these waves from observations during MESSENGER's first six months in orbit.

2. Data Analysis

[8] We searched the full set of MESSENGER Magnetometer [*Anderson et al.*, 2007] data from 3 March to 25 September 2011, or 2.1 Mercury years, for plasma waves within Mercury's magnetosphere at a radial distance of less than 2 R_M from the planet's center. The sampling rate of the Magnetometer data was 20 s^{-1}. Individual fast Fourier transform (FFT) spectra were generated for 20-s segments, over which the data had first been linearly detrended. Successive spectra were stepped 2.5 s in time from one to the

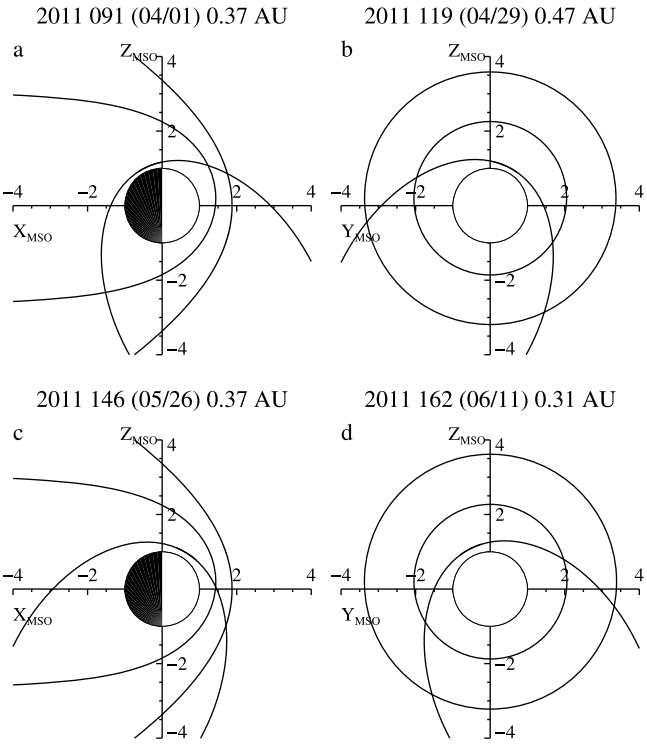

Figure 1. The MESSENGER orbit on days of the year in 2011 when the spacecraft's orbital plane lay approximately in the MSO (a) *X-Z*, (b) *Y-Z*, (c) *X-Z*, and (d) *Y-Z* planes as Mercury orbited the Sun. The orbital trajectory is in the counter-clockwise direction in Figures 1b and 1c and clockwise in Figures 1a and 1d. The radial distance of Mercury from the Sun is given in AU. Also shown are the intersections of the (outer) bow shock and (inner) magnetopause from the model of *Slavin et al.* [2009].

next. For each time and frequency step, polarization parameters (eigenvalues, eigenvectors, ellipticity, degree of polarization or coherency, and wave-normal angles) were computed from the average spectral power matrix. The method we used to compute these quantities is that described by *Means* [1972] and *Arthur et al.* [1976]. With this method, the real part of the spectral power matrix is diagonalized, and the wave-normal direction is given by the eigenvector of the minimum eigenvalue. With the rotation matrices that result from this diagonalization, the complex spectral matrix is then rotated into this diagonalized frame, and the submatrix given by the intermediate and maximum eigenvectors is used to compute the ellipticity and the degree of polarization (DOP). The average spectral power matrix for each frequency and time step is the average of the spectral power matrices over that particular frequency and time step and that of its two nearest neighbors in frequency and six nearest neighbors in time. For this averaging algorithm, we computed the coherency of a white-noise signal to be 0.41 with a standard deviation of 0.15.

[9] The Magnetometer data are in Mercury solar orbital (MSO) coordinates, in which X is directed from the center of the planet toward the Sun, Z is normal to Mercury's orbital plane and toward the north celestial pole, and Y is in the direction opposite to Mercury's orbital motion. The alternative Mercury solar magnetic (MSM) coordinate system is used for computing the magnetic equator, MLT, magnetic latitude, L-shell, and invariant latitude ($\cos^{-1}(1/\sqrt{L})$). The magnetic dipole has been shown to lie nearly along the spin axis, and its location is offset from the planet center along the Z_{MSO} axis by 0.19 R_M [*Anderson et al.*, 2008, 2010, 2011]; i.e., the magnetic equatorial plane is parallel to the MSO *X-Y* plane but is offset by 0.19 R_M in the $+Z_{MSO}$ direction. The transformation from MSO to MSM coordinates is thus simply $X_{MSM} = X_{MSO}$, $Y_{MSM} = Y_{MSO}$, $Z_{MSM} = Z_{MSO} - 0.19\ R_M$.

[10] In addition to waves, MESSENGER frequently detected a constant tone near 0.67 Hz and its second harmonic, neither of which were observed during the flybys. This tone is the result of oscillations of the 3.6-m boom at the end which the Magnetometer sensor is mounted. For small-amplitude boom oscillations in a constant magnetic field, a transverse signal will be generated at the boom oscillation frequency. We examined 10 of these boom oscillation events, and all were associated with slew maneuvers about the spacecraft's *x*-axis, which is aligned with the spacecraft solar panel arms and is perpendicular to the Magnetometer boom [*Anderson et al.*, 2007]. Because the oscillations end abruptly at the end of a maneuver, the boom oscillations are believed to be fed by enhanced jitter from the spacecraft's momentum wheels during the maneuver. The two hinge joints (necessary for deployment) of the boom are oriented in the spacecraft's *y-z* plane, a location that renders the boom susceptible to boom oscillations during spacecraft slews about the *x*-axis. The choice of a 20-s interval for FFT analysis allows us to better separate boom oscillations from magnetospheric waves. Boom oscillations are not included further in our statistical study.

3. Observations

[11] An example of these waves as seen in dynamic spectra computed from the Magnetometer data is shown in Figure 2. On 29 March 2011, the spacecraft encountered narrow-band waves as it approached the magnetic equator from the north. Waves transverse to the local magnetic field were first seen at intermediate magnetic latitudes (starting at ~35°N), and as the spacecraft approached the magnetic equator the wave amplitude increased and the waves shifted to compressional orientations (parallel to the local magnetic field) as the frequency shifted toward f_{cH+}. The fundamental mode and its second harmonic are clearly visible in Figure 2. During this and other wave observations, the fundamental frequency lay between f_{cHe+} and f_{cH+}, and its frequency variation in time was typically smooth. The fundamental frequency often started near or below f_{cHe+} at higher latitudes, rose to f_{cH+} as the spacecraft moved equatorward, and then tended to track f_{cH+} as the spacecraft moved over the southern hemisphere. Similar, highly coherent magnetic waves at frequencies near 1 Hz were nearly always observed (~80% of the equatorial crossings) within Mercury's inner magnetosphere on the nightside, and generally these waves exhibited harmonic banded structure along with a frequency drift in the dynamic spectra.

[12] A segment (50 s long) of the time series of the magnetic field near the magnetic equator (~02:36 UTC) for this example of wave observations is shown in Figure 3. The data have been rotated into directions parallel and

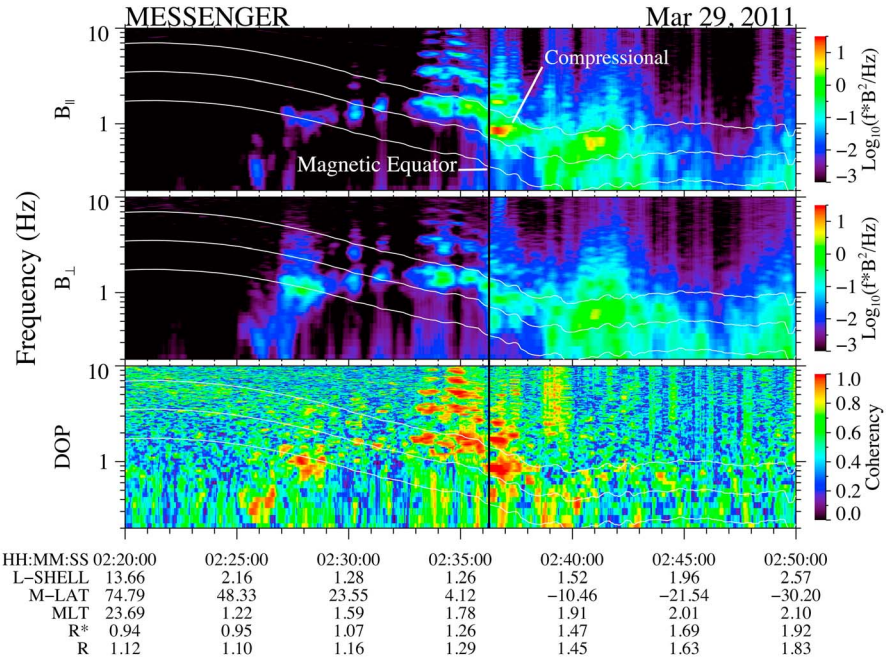

Figure 2. Dynamic spectra of the (top) parallel (compressional) and (middle) perpendicular (transverse) components and (bottom) degree of polarization (DOP) of the magnetic field during the observation of ULF waves at frequencies between 0.2 and 10 Hz following periapsis passage on 29 March 2012. The vertical black line indicates the magnetic equator. The white curves show the (top to bottom) H^+, He^{++}, and He^+ cyclotron frequencies. The time-axis label L-SHELL is the magnetic L-shell, M-LAT is magnetic latitude in degrees, MLT is magnetic local time in hours, R is the radial position of the spacecraft from planet center in R_M, and R^* is the radial distance from the offset dipole. Narrow-band harmonic waves are observed in all panels. The waves are highly compressional (see Figure 3) near the magnetic equator and transverse away from the magnetic equator.

perpendicular to the average local magnetic field during this interval. Two-dimensional minimum variance analysis (MVA) has been performed on the two components in the perpendicular plane; $B_{\perp 1}$ points in the minimum variance direction in that plane, and $B_{\perp 2}$ points in the maximum variance direction in that plane. The compressional $B_{\|}$ component dominates, with a maximum peak-to-peak amplitude of ∼10 nT in an ambient field of 84 nT, indicating that the wave magnetic field components are strongly linear and parallel to the local field. The compressional component is highly distorted from a sinusoidal waveform, consistent with the multiple harmonics observed in Figure 2. A mild magnetic depression marks the crossing of the plasma sheet near the equatorial crossing.

[13] For a substantial minority (∼25%) of the wave events, the compressional component was not dominant near the magnetic equator but instead the transverse component was larger. An example of such an event on 1 August 2011 is shown in Figure 4. During this event the transverse component dominated throughout, from 09:09 to 09:25 UTC. A time series of the largest-amplitude waves, about ∼6 nT peak-to-peak oscillation in a 90 nT ambient field, is shown in Figure 5. The near sinusoidal signal observed in all three components makes this an ideal event for MVA. A hodogram of the intermediate (B_2) and maximum (B_3) variance components of this time series is given in the inset in Figure 5. The ratio of intermediate to minimum eigenvalue is 12, which yields a well-determined wave-normal angle (WNA) of 35°. The waves at the magnetic equator are left handed with respect to the ambient magnetic field and have an ellipticity of −0.35, which is suggestive of the ion cyclotron mode. However, MVA applied to a few wave cycles at a time away from the equator yielded mixed results, with both left- and right-handed polarization. Near the equator, the orientation of the major axis is perpendicular to our estimate of the gradient in the magnetic field magnitude. However, this example is an exception in that even events that are dominantly transverse at the equator tend to be highly linear. For the data set analyzed for this paper, only two other orbits were identified with strong transverse oscillations at the equator; for both such events the major axis of the polarization ellipse was also perpendicular to our estimate of the gradient of the magnetic field magnitude.

[14] We did not clearly detect waves in the tail at distances $R > 2\ R_M$, in settings for which the orbit was similar to that of Figure 1c. A few examples of two to four cycles of low-amplitude oscillations at a frequency near 1 Hz were observed in the tail at such distances. A statistical analysis of the distribution of observed waves, presented next, is followed later in the paper by a brief discussion of possible reasons why these waves are not seen deeper in the tail.

4. Statistics

[15] The overall coverage of the wave observations is shown in Figure 6. Average integrated power spectral

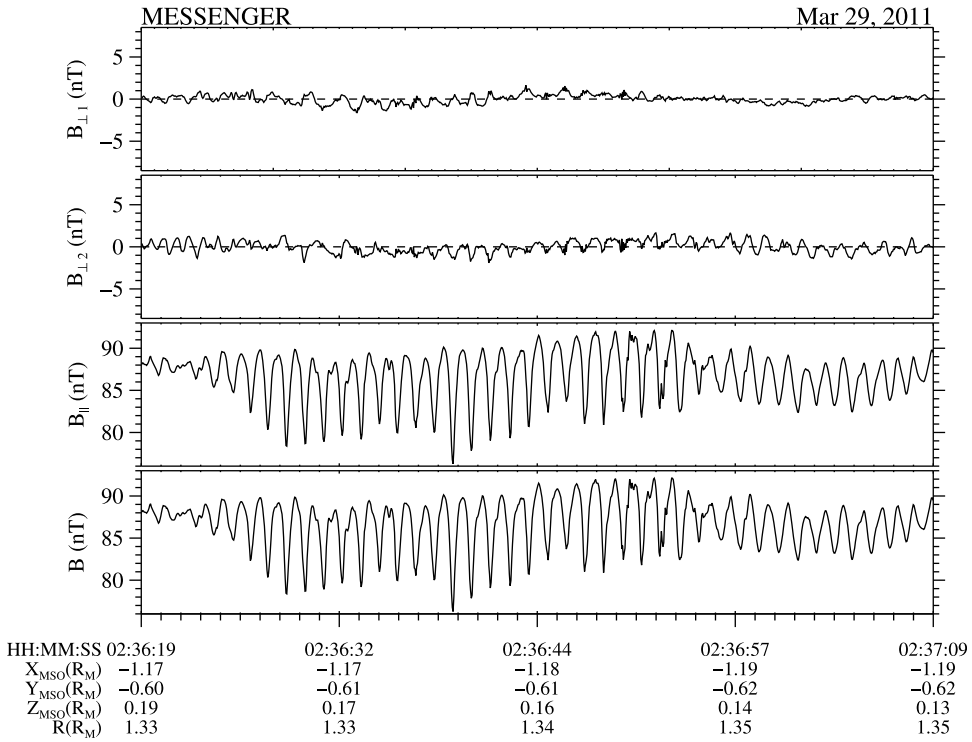

Figure 3. Strongly compressional waves near the magnetic equator for a portion of the data set depicted in Figure 2. The first and second panels are the perpendicular components of the field (see text), the third panel is the parallel component, and the fourth panel is the field magnitude. Peak-to-peak amplitudes are ~10 nT.

density between 0.8 and 5.0 Hz binned by magnetic latitude and MLT is shown in Figure 6a. Because of MESSENGER's orbit and the proximity of Mercury's dayside magnetopause to the planet, there was no Magnetometer coverage near the dayside magnetic equator. The plot shows clear enhancements in intensity in two regions. One is more or less centered about the magnetic equator, the result of these narrow-band ULF waves, and is concentrated on the nightside (18 to 6 h MLT). The second is in the cusp region (9 to 14 h MLT at magnetic latitude >40°). From visual inspection of the dynamic spectrum in the cusp region, the magnetic fluctuations in the cusp region tend to be broadband.

[16] We visually examined each dynamic spectrogram for each orbit in the data set, and we marked regions in time and frequency at which narrow-band waves were observable, taking care to exclude boom oscillations. Within each marked region the following criteria were used to identify wave events: (1) DOP >0.90 (about three standard deviations above the white-noise level); (2) the power spectral density >0.2 nT^2/Hz; and (3) the power spectral density was more than two standard deviations above the estimated background of the spectrum. Of the frequencies at which these criteria were satisfied, the frequency at maximum power was retained for each time step. With these criteria about 21,000 wave events were identified. The distribution of those events in MLT and magnetic latitude is shown in Figure 6b. The waves were detected at all MLTs, but they were concentrated on the nightside. For the wave events near midnight MLT the orbital configuration was similar to that shown in Figure 1a, and the waves occurred mainly in northern hemisphere regions where the magnetic field lines were most likely closed. From an MLT of 20 h to an MLT of 14 h in Figure 6b the distribution of events shows a tendency to split into two branches, one near the magnetic equator and another that rises to higher latitudes from dusk to noon. This apparent splitting was seen in both Mercury years. A similar splitting is seen between MLT noon and dusk.

[17] The location of plasma sheet crossings during this period for $R_M < 2$ is indicated in Figure 6c. As expected these crossings are located on the nightside, and the highest concentration is seen around midnight. Plasma sheet intervals are identified as regions in which the magnetic field strength is at least 10 nT less than the adjacent tail-lobe field strength. The plasma sheet was encountered only on about half of the nightside crossings of the magnetic equator. A similar distribution of plasma sheet locations was given by *Korth et al.* [2011].

[18] Histograms of the number of wave events as a function of MLT, magnetic latitude, and radial distance are given in Figures 7a–7c. For normalization, the number of time samples in the data set is given as a function of MLT and magnetic latitude in Figures 7d–7f. In Figures 7g–7i the number of events (Figures 7a–7c) is shown normalized by respective coverage (Figures 7d–7f). The distribution of wave events with MLT drops off strongly on the dayside, but this pattern is at least in part the result of the lack of coverage near the dayside magnetic equator as well as broadband turbulence in the cusp region masking these waves if they occur. The distribution of events peaks near the magnetic equator (magnetic latitude 10 ± 18°). The distribution of events peaks at a radial distance of (1.35 ±

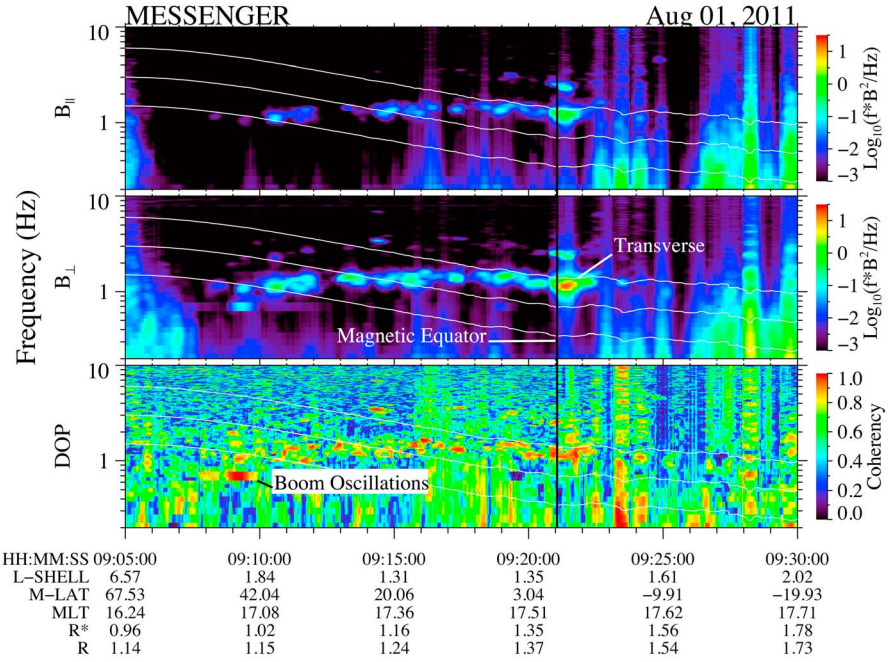

Figure 4. An example of a ULF wave for which the transverse component was dominant at all latitudes, even during equatorial passage. In addition to the magnetospheric waves, oscillations of the Magnetometer boom induced by spacecraft attitude adjustments are visible at a frequency of ∼0.7 Hz at 9:08 UTC.

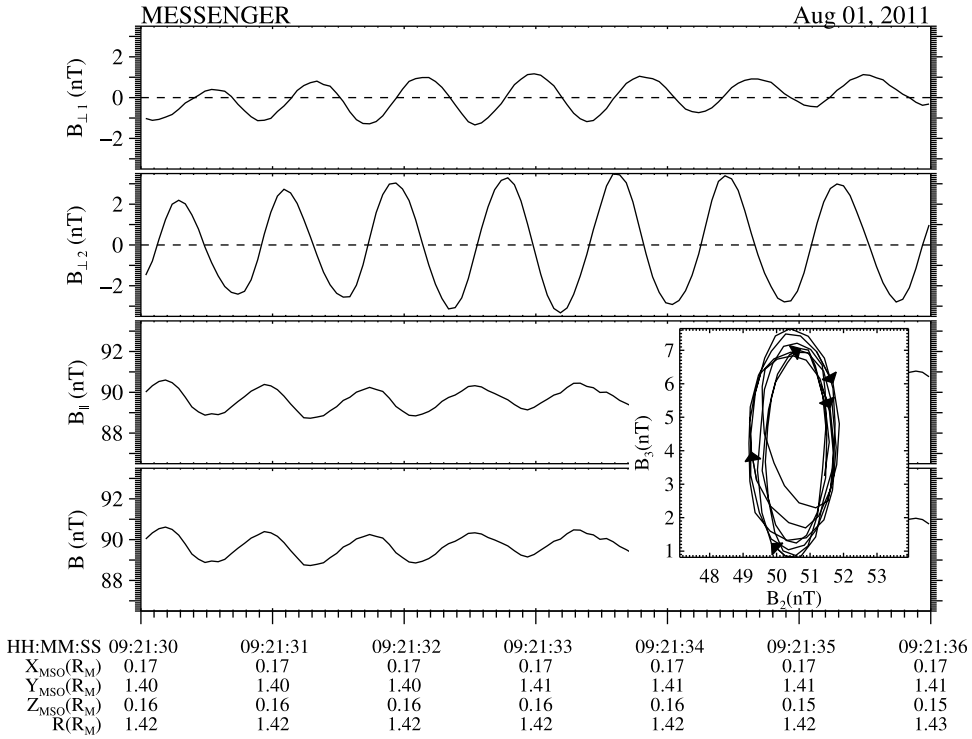

Figure 5. Strongly transverse waves near the magnetic equator for a portion of the data set depicted in Figure 4. Maximum peak-to-peak amplitudes are ∼6 nT. Inset: Hodogram of the intermediate (B_2) and maximum (B_3) variance components of the time series. The major axis of the polarization ellipse is perpendicular to the estimated gradient in field magnitude. The wave frequency f is ∼1.1 Hz, the ratio f/f_{cH+} is ∼0.8, the WNA is ∼35°, and the waves are left handed with an ellipticity of −0.35.

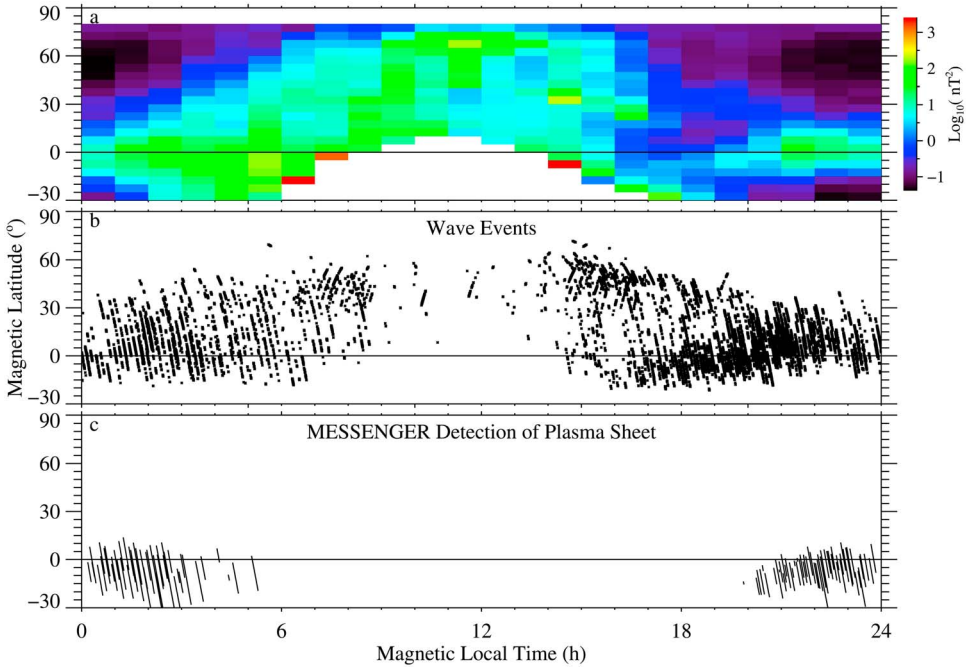

Figure 6. Coverage in magnetic latitude and magnetic local time from 24 March–25 September 2011, for periods when the spacecraft was inside Mercury's magnetosphere and $R < 2\ R_M$. (a) Integrated spectral power over frequencies between 0.8 and 5.0 Hz for all data during this period (both with and without waves). (b) Observed wave events versus magnetic latitude and magnetic local time. Note the bifurcation in latitude of the distribution between dawn and noon and again from 20 h MLT toward dusk. (c) Plasma sheet crossings versus magnetic latitude and magnetic local time.

0.13) R_M. The frequency of events drops toward zero as the radial distance increases toward 2 R_M.

[19] Histograms of several characteristics of the wave events are given in Figure 8. A histogram of wave frequency (Figure 8a) shows three distinct peaks: one at a frequency just below f_{cHe++}, a dominant peak at a frequency just below f_{cH+}, and a peak near the second harmonic of that frequency at $\sim 2f_{cH+}$. A histogram of the ratio of power in the parallel component to the total power (Figure 8b) indicates that the number of compressional events approximately equals the number of transverse events. If the DOP selection criterion is raised above 0.90, the distribution of events becomes skewed toward the compressional side (1.0), and if the DOP selection criterion is reduced below 0.90 the distribution of events becomes skewed toward the transverse side (0.0). A histogram of wave ellipticity (Figure 8c) indicates that the waves tend to be linear, with ellipticity peaked near zero (0.10 ± 0.37) and with some bias toward right-handed polarization. A histogram of wave-normal angles (Figure 8d) shows a peak near 90°. There is also a small peak near ~10°. For transverse events that are strongly linear, the error in the wave-normal angle is large and contributes to the broad distribution observed at angles between 0° and 75°.

[20] One of the most dominant features of the distribution of wave events is that the waves are strongly compressional near the magnetic equator and strongly transverse far from the equator. This pattern can be seen in a plot of the ratio of parallel-component power to total power for nightside events (Figure 9a). Near 0° latitude, most values of this power ratio exceed 0.7; as the DOP selection criterion is raised this tendency is strengthened, whereas as the DOP selection criterion is lowered this tendency is weakened. The total power in the wave events also maximizes around the equator and drops off with increasing magnetic latitude, as shown in Figure 9b.

[21] The average wave frequency and magnetic field strength for the 969 events inside the plasma sheet is 0.90 ± 0.36 Hz and 59 ± 13 nT, respectively. In contrast, the average wave frequency and magnetic field strength of the 8625 nightside wave events within 10° of the magnetic equator but on orbits that did not encounter the plasma sheet is 1.27 ± 0.6 Hz and 86 ± 20 nT, respectively. The average power spectral density in the plasma sheet is about a factor of 2 larger than that outside at similar latitudes. This finding is qualitatively consistent with that of the flybys. The average ratio of the compressional to total wave power is 0.6 near the equator for both the flybys and orbital crossings.

[22] A plot of ellipticity versus magnetic latitude for wave events that are strongly transverse (ratio of power in the perpendicular component to total power >0.7) is shown in Figure 9c. Near the magnetic equator the absolute value of the ellipticity is ~0.5, whereas at higher magnetic latitudes the absolute value of the ellipticity decreases toward 0 as the waves become more strongly linear. Shown in Figure 9d is a histogram of the angle (ζ) between the maximum eigenvector direction and the estimated direction of the magnetic field gradient for those events for which the angle between the maximum eigenvector direction and the local magnetic field direction is greater than 70° and the magnetic latitude is greater than 20°. The median of ζ is 70°, a value suggesting that far from the magnetic equator the maximum wave

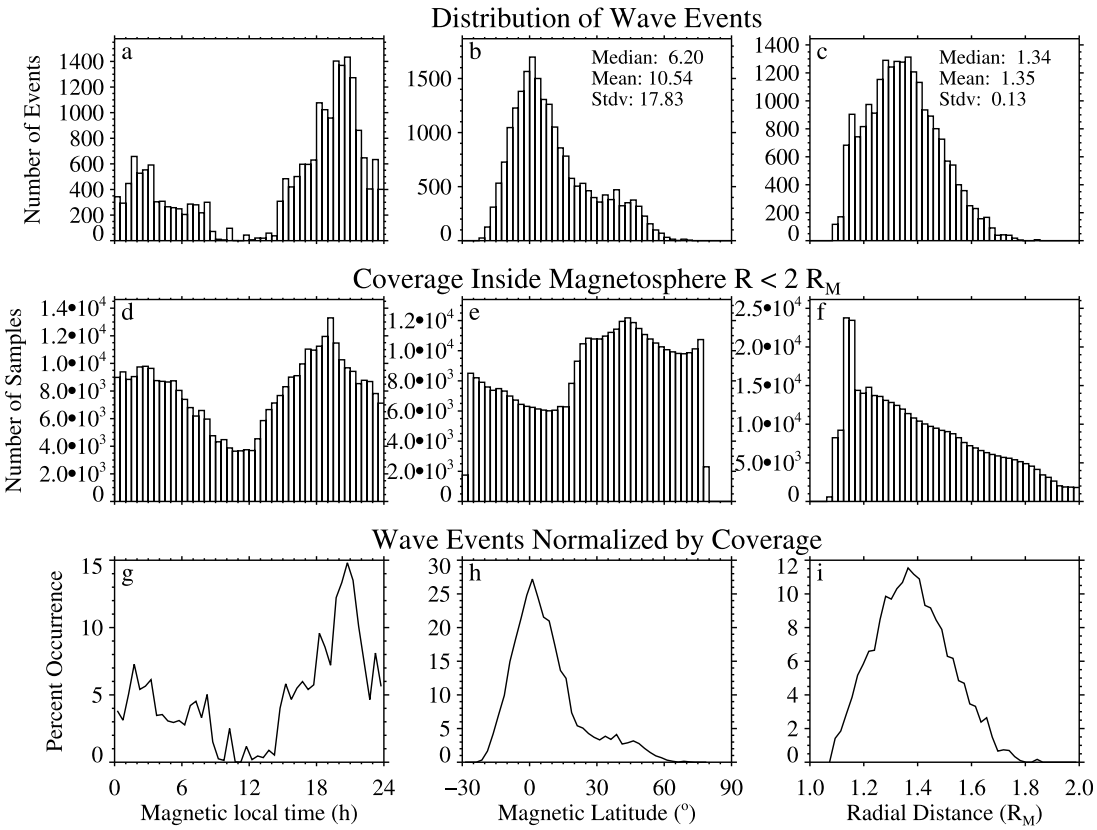

Figure 7. Histograms of wave events as a function of (a) magnetic local time, (b) magnetic latitude, and (c) radial distance; coverage in (d) MLT, (e) magnetic latitude, and (f) radial distance; (g–i) wave events from Figures 7a–7c normalized by their respective coverage from Figures 7d–7f. The total number of time samples with wave events is 21,482 for Figures 7a–7c, and the total number of samples is 381,981 for Figures 7d–7f. The percent occurrences in Figures 7g–7i correspond to bin sizes of 0.5 h, 2.5° latitude, and 0.02 R_M radial distance, respectively. In Figures 7b and 7c median, mean, and standard deviation (Stdv) are also given.

magnetic field fluctuations are nearly perpendicular to the background magnetic field gradient.

5. Discussion

[23] The plasma and magnetic field properties of Mercury's inner magnetosphere provide important context to the wave observations reported in this paper. Mercury occupies a large fraction of the volume of this region; scaled to Earth's magnetosphere the surface of Mercury would be at radial distance of 8 R_E [*Slavin et al.*, 2008], where R_E is Earth's radius. This large volume fraction filled by the planet means that on the dayside there is no minimum in magnetic field magnitude at the magnetic equator [*Alexeev et al.*, 2008] and that on the nightside the true magnetic equator (the point along a field line at which the background magnetic field strength is a minimum) can have large fluctuations about the mean position in response to changing solar wind conditions. Because compressional waves tend to be confined near magnetic field minima [see *Boardsen et al.*, 1992, Figures 4–6], they should not be observed at low latitudes on the dayside if generated locally. Also the transition from compressional to transverse (Figure 9a) waves with increasing magnetic latitude can be understood at least qualitatively in terms of the confinement of compressional waves about the magnetic field minimum. Because the plasma at Mercury has multiple ion species, as transverse-dominant plasma waves (Figure 9c) move away from the equator into regions of increasing field strength the ratio of wave frequency to f_{cH+} decreases and waves approach a plasma crossover frequency (e.g., between f_{cH+} and f_{cHe++}, or between f_{cHe++} and f_{cNa+}). As waves approach such a crossover frequency they become more linear [*Gurnett et al.*, 1965; *Rauch and Roux*, 1982; *Stix*, 1992]. This explanation at least qualitatively allows one to understand the trend in the absolute value of the ellipticity (Figure 9c), which decreases toward zero (linear waves) with distance from the magnetic equator. Electromagnetic ion cyclotron waves (ICWs), which have ellipticity <0, should be guided along a magnetic field line [*Rauch and Roux*, 1982], but for the results in this paper there is a skew toward right-handedness, even for transverse-dominant waves (Figure 9b). Unless there are field-aligned mass density irregularities present, these waves will not follow the field line. For a source that is distributed in space for non-ducted waves, wave spectra would be broadband away from the source, in contrast to the narrow-band spectra that are observed. We note, however, that the observation of right-handed transverse waves could be due to the limitations of the standard polarization analysis used in this study.

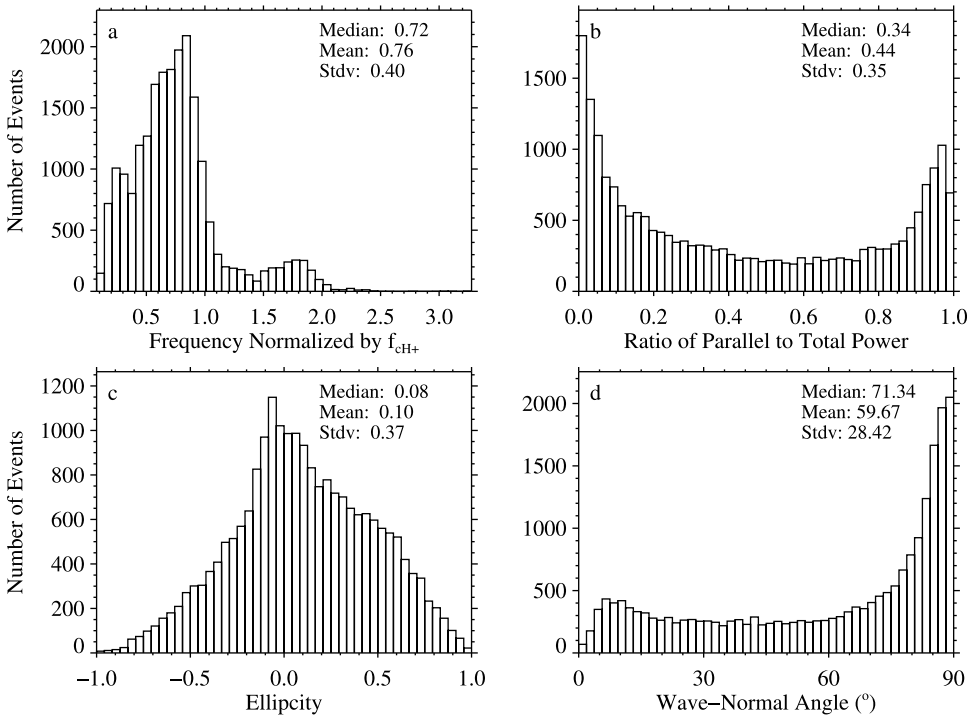

Figure 8. Histograms of wave events as a function of (a) frequency, normalized by the proton cyclotron frequency, (b) ratio of the parallel power to total power, (c) ellipticity (−1 is left-handed circular, 0 is linear, and 1 is right-handed circular polarized with respect to the background field), and (d) wave-normal angle. A total of 21,482 samples was used for each histogram.

[24] Polarization analysis works best when one dominant wave mode is present. When two or more modes are competing for dominance, their superposition renders difficult the interpretation of wave-normal angle and ellipticity derived from such analysis [*Anderson et al.*, 1996; *Denton et al.*, 1996]. *Denton et al.* [1996] investigated the case when two ICW modes are present with identical frequencies, amplitudes, ellipticities, and wave-normal angles. For this case the only free parameters are the angle $\delta\alpha$ between the minor axes of the two polarization ellipses and the relative phase $\delta\varphi$ between the two modes. *Denton et al.* [1996] showed that, as these two parameters are varied, wide ranges in wave-normal angle and ellipticity can result from the polarization analysis of the superposed waves, even for solutions with positive ellipticity.

[25] If the transverse waves reported here are field-aligned resonances (i.e., standing waves constructed from ICWs), they can be regarded as a superposition of two ICWs propagating in opposite directions, similar to the model of *Denton et al.* [1996]. For ICWs with a wave-normal angle of 0° (i.e., purely left-circularly polarized), their superposition will always yield left-circularly polarized waves. For nonzero wave-normal angles, however, part of ($\delta\alpha$, $\delta\varphi$) phase space will yield right-handed solutions from polarization analysis. We repeated the two-wave superposition analysis of *Denton et al.* [1996] using as input a wave-normal angle of 35° and an ellipticity −0.35 (from the left-handed waves shown in the inset of Figure 5). In that analysis 84% (16%) of ($\delta\alpha$, $\delta\varphi$) phase space yielded negative (positive) ellipticity values with a normalized median power of 0.68 (0.32). We compared this outcome with the data points in Figure 9c for magnetic latitudes between 0° and 15°, where there is a clear bifurcation in the ellipticity values. Of these points, 362 have negative ellipticity with a median power of 0.38 nT^2/Hz, and 1099 have positive ellipticity with a median power of 0.25 nT^2/Hz, i.e., 25% (75%) of the data points have negative (positive) ellipticities with a normalized median power of 0.60 (0.40).

[26] The median power indicated by polarization analysis of both the observations and the results from the two-wave superposition model is larger for left-handed than right-handed ellipticities. This difference can be understood as the superposition of two left-handed wave modes, each of which can be regarded as a superposition of a larger-amplitude left-handed circular trace and a smaller-amplitude right-handed circular trace. So, in order to add two such left-handed wave modes to obtain a right- (left-) handed solution from the polarization analysis of the sum of two left-handed waves, the two larger (smaller) left- (right-) handed traces must nearly cancel out to yield a smaller- (larger-) amplitude solution. A total of 84% of the phase space was left handed in the analysis of superposed model waves, compared with only 25% of the data points. This difference might be attributable to non-uniform sampling of ($\delta\alpha$, $\delta\varphi$) phase space, with both $\delta\alpha$ and $\delta\varphi$ constrained by the reflection of these waves off Mercury or because of approach to an ion-ion resonance along the field line. Although more work is needed on this topic, the transverse waves reported here may be primarily left handed rather than a mixture of right- and left-handed waves as indicated by the results of standard polarization analysis.

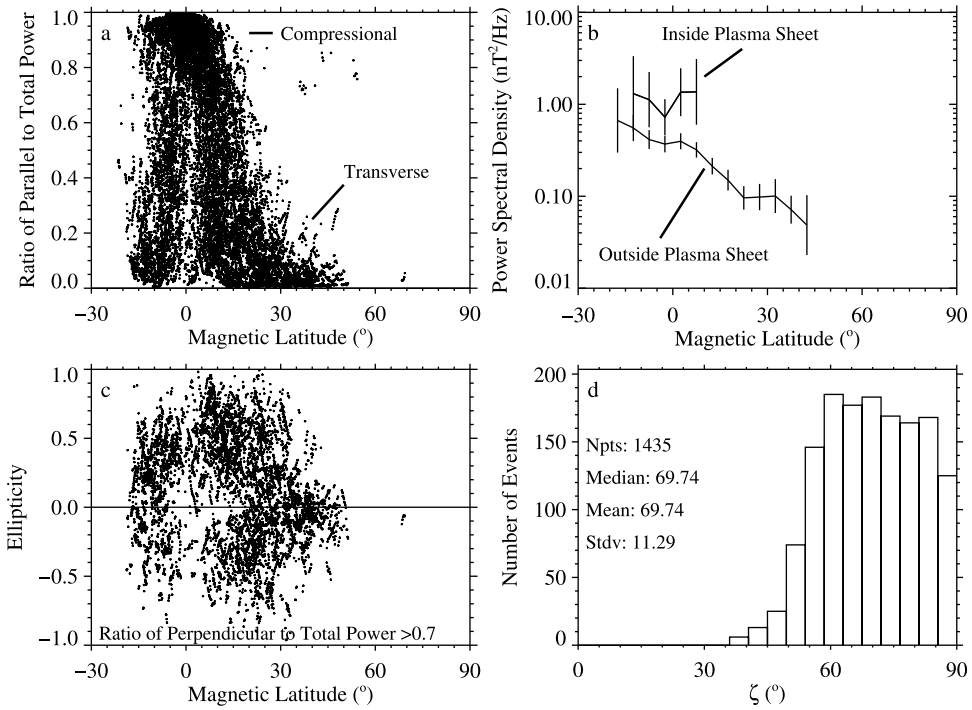

Figure 9. (a) Ratio of parallel power to total power versus magnetic latitude for nightside wave events. The waves tend to be compressional near the equator and strongly transverse away from the equator. (b) Average power spectral density of nightside wave events versus magnetic latitude, distinguished on the basis of position relative to the plasma sheet. (c) Wave ellipticity versus magnetic latitude for wave events for which the ratio of transverse power to total power is greater than 0.7. (d) Histogram of the angle (ζ) between the direction of the maximum eigenvector and the estimated direction of the gradient in the local magnetic field, for those events for which the angle between the maximum eigenvector direction and the direction of the local magnetic field is greater than 70° and the magnetic latitude is greater than 20°.

[27] The observation that, far from the magnetic equator, the direction of the maximum eigenvector for wave magnetic field variation is nearly perpendicular to the background magnetic field gradient (Figure 9d) is strongly suggestive that there is a substantial component of field-aligned resonances to these wave observations. At frequencies below the lowest cyclotron frequency in the Alfvén resonator frequency range, simulations predict that at the point where compressional waves couple with transverse waves the transverse magnetic field component of the wave will be strongly perpendicular to the background magnetic field gradient [*Zhu and Kivelson*, 1989]. This behavior is also predicted for mode coupling at the ion-ion hybrid resonance [*Kim et al.*, 2008].

[28] In a simulation with a constant background magnetic field, *Kim et al.* [2008, Figure 4] showed that compressional waves are mode converted to transverse waves for which the dominant transverse magnetic field component is perpendicular to the mass density gradient. The coupling occurs at the H^+–Na^+ hybrid resonance at a frequency of 0.2 f_{cH+}. Moreover, *Kim et al.* [2011, Figure 1b] determined the H^+–Na^+ hybrid resonance and its first two harmonics versus fractional composition of Na^+ in a H^+–Na^+ plasma. From the theory of *Kim et al.* [2011] we may estimate the Na^+ fractional composition for the event shown in Figures 4–5. At the magnetic equator the observed f/f_{cH+} ratio is ~0.8; at that value of the ratio in *Kim et al.* [2011, Figure 1b], their theory predicts that the fractional composition of Na^+ is 0.8, 0.9, and 0.95 for the first three harmonics, respectively. A few estimates of the Na^+ ratio have been determined in Mercury's near magnetosphere from measurements made by MESSENGER's Fast Imaging Plasma Spectrometer (FIPS) during the Mercury flybys [*Raines et al.*, 2011] and from orbit [*Zurbuchen et al.*, 2011]. These estimates, summarized in Table 1, span the range 0.08 to 0.52, values lower than the values of 0.8 to 0.95 predicted by the *Kim et al.* [2011] simulations. The median value of the ratio f/f_{cH+} for all wave events analyzed here is 0.72 (Figure 8a), a value that suggests a larger fractional composition of Na^+ than what has been reported from analysis of the plasma ion data to date. However, an additional ion species added to the plasma, e.g., He^{++}, would modify the ion-ion resonances, e.g., the H^+–He^{++} and He^{++}–Na^+ hybrid resonances would

Table 1. FIPS Observations in Mercury's Plasma Sheet[a]

Flyby	n_{H+} (cm^{-3})	T_{H+} (eV)	% Na^+	Reference
M1	1 to10	170 eV	15	*Raines et al.* [2011]
M2	4 to 5	690 eV	8	*Raines et al.* [2011]
In orbit	1.6 and 0.28	310 and 670	11 and 52	*Zurbuchen et al.* [2011]

[a]The quantity n_{H+} is the proton density, T_{H+} is the proton temperature, and % Na^+ is the fractional contribution to the plasma pressure by Na^+-group ions and is derived under the assumptions that there is pressure balance between the plasma sheet and adjacent lobes and that $T_{H+} \sim T_{Na+}$ [*Raines et al.*, 2011].

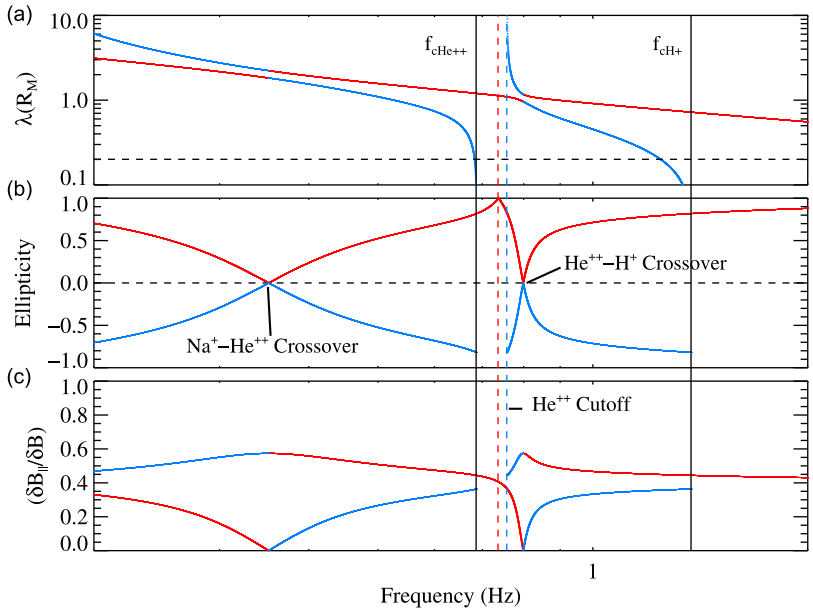

Figure 10. (a) Wavelength λ, (b) ellipticity, and (c) ratio of the wave compressional field ($\delta B_{\|}$) to the total wavefield (δB) versus frequency for a wave-normal angle of 35° in a background field of 90 nT. The plasma density is 1 cm^{-3} and the fractional ion composition is 0.86 H^+, 0.05 He^{++}, and 0.09 Na^+. The crossover frequencies are indicated along with f_{cHe+} and f_{cHe++}. Blue denotes left-handed polarization, and red denotes right-handed polarization.

replace the H^+–Na^+ hybrid resonance. For wave frequencies observed between f_{cHe++} and f_{cH+} one would predict the fractional composition of He^{++} as opposed to that of Na^+.

[29] If these transverse waves are field-line resonances composed of ICWs, how do the wavelengths compare with the length of the field line? From cold-plasma theory we have estimated the wavelengths, ellipticities, and compressional field in Figure 10. The wave-normal angle and background field are from Figure 5, but plasma density and ion composition are not known, so we adopted 1 cm^{-3} for the plasma density and assumed that the plasma is composed of H^+, He^{++}, and Na^+. The ratio of He^{++} to H^+ is taken to be 5%, a typical solar wind value, and the ratio of Na^+ to total ions is assumed to be 9% (see Table 1). The observed wave frequency in Figure 5 is 1.1 Hz, which gives a wavelength for the left-handed mode in Figure 10 of 0.34 R_M and an eccentricity of −0.75. The approximate condition for a field-line resonance is $2l_{DIP}/\lambda_{\|} = n$, where n is an integer, l_{DIP} = 1.8 R_M is the length of the dipole field line, and $\lambda_{\|}$ is the parallel wavelength. For a wavelength of 0.34 R_M the field-line resonance harmonic number n is ~8, which is large. Note that the observed ellipticity of −0.35 from Figure 4 is smaller than −0.75 from Figure 10. A number of parameters can be changed to lower the magnitude of the model ellipticity, such as increasing the wave-normal angle, He^{++} concentration, or Na^+ concentration. For demonstration purposes we do the last. When the Na^+ concentration is raised to 55% and the ratio of He^{++} to H^+ is held fixed, the ellipticity becomes −0.37, the wavelength increases to 1.77 R_M, and the harmonic number n of the resonance is ~2. Therefore it is plausible that these transverse waves could be field-line resonances.

[30] The above arguments are based on cold-plasma theory, which is valid only for low values of the ratio β of plasma pressure to magnetic pressure. Because Mercury has no ionosphere and a low rotation rate, it is not thought to have a cold-plasma component inasmuch as there is no co-rotational electric field required to trap cold ions and no ionosphere that could serve as a source of low-energy ions. The ion plasma parameters at Mercury are important in understanding the plasma wave phenomena. Because of the limited field of view of the sensor, however, plasma parameters have been estimated from FIPS measurements only for a limited number of intervals when MESSENGER was in Mercury's plasma sheet during the Mercury flybys [*Raines et al.*, 2011] or in orbit [*Zurbuchen et al.*, 2011]; see Table 1. A determination of the relative composition H^+ and Na^+ is derived from the assumption of pressure balance between the magnetic pressure and particle pressure in the plasma sheet and lobes. From these parameters as well as typical values of the magnetic field magnitude B observed in the plasma sheet, we show in Table 2 estimates of the proton beta β_{H+} derived from the ratio of estimated proton thermal speed C_{H+} to the Alfvén speed V_A and the relation $\beta_{H+} = (C_{H+}/V_A)^2$.

[31] A number of factors could explain the drop off in the occurrence of wave events with radial distance (Figure 7c).

Table 2. Estimates of β_{H+} for Several Combinations of Plasma Density n_e and Fractional Ion Composition From Table 1

B (nT)	n_e (cm^{-3})	% H^+	% Na^+	V_A (km/s)	C_{H+} (km/s)	C_{H+}/V_A	β_{H+}
60	5	100	0	590	170–250	0.3–0.4	0.09–0.16
60	5	90	10	330	170–250	0.5–0.8	0.25–0.64
60	5	50	50	170	170–250	1.0–1.4	1.0–2.0
60	1	100	0	1320	170–250	0.13–0.19	0.02–0.04
60	1	90	10	740	170–250	0.22–0.34	0.05–0.12
60	1	50	50	380	170–250	0.45–0.67	0.2–0.45

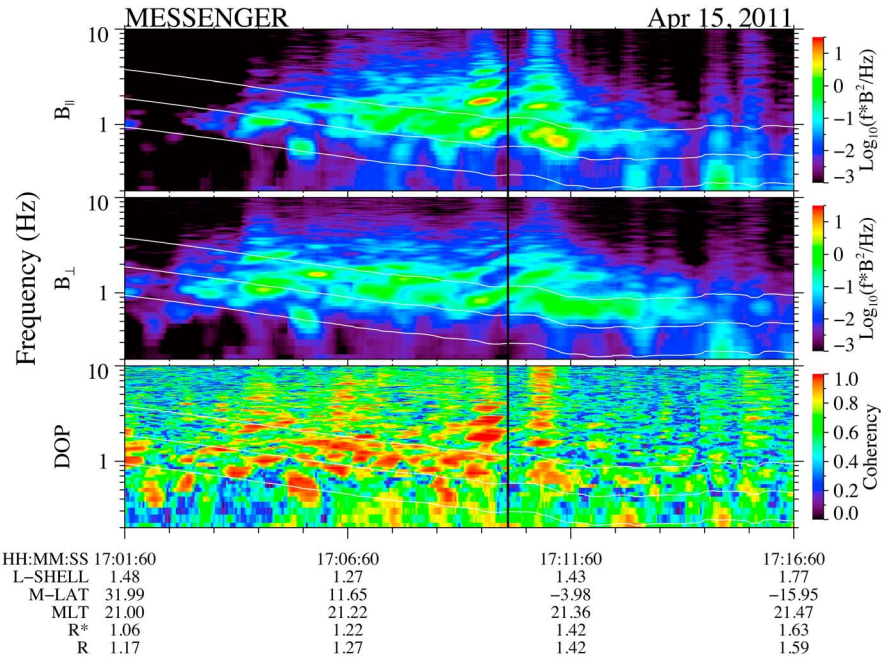

Figure 11. A spectrogram (in the same format as Figures 2 and 4) that displays two intensity enhancements, mainly compressional and dominantly in the first two harmonics, which straddle the magnetic equator (black vertical line). The ratio of the fundamental frequency to f_{cH}^{+} is ~0.7.

If these waves are field-line resonances they will occur on closed field lines and the number of closed field lines will decrease with increasing radial distance down the tail. Near midnight these waves are not observed above an invariant latitude of 40°, which could indicate a boundary between open and closed field lines on the nightside. Another explanation is that a substantial number of protons are in bounce resonance with the wave period. In a dipolar field, 500 eV protons will be in bounce resonance with the equatorial proton cyclotron period at an L-shell of 3. If the proton temperature is 500 eV, there will be a substantial number of protons near 2 keV energy that will be in bounce resonance with the equatorial cyclotron period at an L-shell of 2. If these waves are generated locally by a loss cone instability, then from an L of 1.1 to 2 the planetary loss cone angle will decrease from 67° to 20°, providing a free energy source for the instability that decreases with increasing L-shell [e.g., *Schriver et al.*, 2011].

[32] The mean radial location of these waves of 1.35 R_M (Figure 7c) corresponds to a distance of 10.7 R_E in Earth's nightside magnetosphere. Narrow-band waves near the proton cyclotron frequency have recently been reported in Earth's plasma sheet boundary layer [*Engebretson et al.*, 2010] at distances of 8 to 18 R_E in the tail, and both beam and ring (shell) proton velocity distributions were observed during these events. The frequency–time structure of these spectra is similar to that for the waves observed at Mercury, except that the waves at Earth are transverse dominant. From an instability analysis of these waves, *Denton et al.* [2010] concluded that they are generated by proton ring (shell) distributions for large β_{H+}. For $\beta_{H+} \sim 0.4$ the waves are electromagnetic transverse dominant, and as β_{H+} increases they remain electromagnetic but become compressional when $\beta_{H+} \sim 2$ [*Denton et al.*, 2010]. *Gary et al.* [2010] pointed out that this wave mode is the electromagnetic ion Bernstein mode. Whereas *Denton et al.* [2010] adopted an anisotropic ring distribution, *Gary et al.* [2010] modeled the same instability with an isotropic ring distribution for $\beta_{H+} \sim 0.5$ and obtained nearly identical growth rates to those of *Denton et al.* [2010], suggesting that anisotropy is not important for this instability. *Gary et al.* [2010] did not explore the instabilities at $\beta_{H+} \sim 2$, at which the waves became compressionally dominant [*Denton et al.*, 2010]. In both studies f/f_{cH+} at maximum growth rate was very close to 1 and the wave-normal angle was near 90°; *Gary et al.* [2010] computed a wave-normal angle of 86° at maximum growth rate. *Denton et al.* [2010] found that these waves are highly linear and cited a typical ellipticity of 0.02. In our statistical study the median values from Figure 8 are 0.72 for f/f_{cH+}, 0.08 for ellipticity, and 71° for the wave-normal angle. Given the limitations of polarization analysis these values are consistent with the electromagnetic ion Bernstein mode. *Gary et al.* [2010] showed further that the fundamental mode does not always dominate. In our study the fundamental mode is usually but not always the dominant harmonic; in Figure 11, for instance, the power in the 2nd harmonic is larger than that of the fundamental mode just prior to the magnetic equator crossing. An approximate estimate of the wavelength λ of the fundamental mode can be made from the relation [*Gary et al.*, 2010, Figure 4] $\lambda \sim V_1/(3f_{cH+})$, where V_1 is the ring velocity. For a ring velocity equal to a proton thermal speed of 210 km/s and a 60 nT field, the wavelength is ~80 km. If these waves correspond to the electromagnetic ion Bernstein mode, their wavelengths are much smaller than the dimension of Mercury's magnetosphere.

[33] For the waves represented in Figure 9a the average background magnetic field energy density increases with increasing magnetic latitude. If the proton energy density is constant on average over this range of magnetic latitude, then β_{H+} will decrease with increasing magnetic latitude. If these waves are mainly composed of electromagnetic ion Bernstein modes, then as β_{H+} decreases they will transition from compressional to transverse dominant [*Denton et al.*, 2010]. Therefore, the transition from compressional to transverse dominance as magnetic latitude increases (Figure 9a) can be qualitatively understood if these waves are electromagnetic ion Bernstein modes in a high-β_{H+} plasma for which β_{H+} decreases with increasing magnetic latitude. Further experimental and theoretical analysis is warranted to explore this possible interpretation.

[34] Shell distributions observed deep in Earth's plasma sheet boundary layer (as opposed to the shell distributions observed near and inside geosynchronous orbit at Earth [*McIlwain*, 1972] for which a co-rotational electric field is required, unlike the situation at Mercury) are believed to be generated by counterstreaming protons that are scattered in pitch angle [*Engebretson et al.*, 2010]. Observations of such distributions at Mercury have not been reported, and whether a similar mechanism occurs in Mercury's plasma sheet boundary layer that would generate proton shell distributions has not been explored. However, the strong loss cone distributions predicted to occur in Mercury's inner magnetosphere could provide the positive perpendicular slope necessary for the generation of waves for this β_{H+}-dependent instability. Figure 11 shows a spectrogram for an event characterized by two intensity enhancements that are mainly compressional and are observed to straddle the magnetic equator. These events could be interpreted as waves generated by local instabilities during two crossings of the plasma sheet boundary layer, although the location of the plasma sheet and its boundary layers are not clear from only the Magnetometer data for this event.

[35] The observation that the wave power is maximum at the equator and is a factor 2 larger in the plasma sheet suggests that the waves reported in this study are due to a local plasma instability. The increase in power at the equator could be attributed to the focusing of compressional waves from the magnetopause, but we believe that this focusing would produce a broadband spectrum rather than the narrow-band spectra that are observed. If field-line resonances exist, they could be driven by local instabilities, in contrast to compressional waves that are generated remotely at the magnetopause. Linear stability analysis using a loss cone distribution in high-β_{H+} plasma is required to determine if loss cone distributions can generate both transverse and compressional electromagnetic waves with changing β_{H+}.

6. Conclusions

[36] This paper has presented a survey of highly coherent ULF waves at frequencies between 0.4 and 5 Hz in Mercury's inner magnetosphere ($R < 2\ R_M$). The survey covers the time period from 24 March to 25 September 2011, or 2.1 Mercury years. These waves usually exhibit banded harmonic structure that drifts in frequency as the spacecraft traverses the magnetic equator. These waves are observed at all MLTs, but their occurrence strongly drops off on the dayside, which is partly due to orbital bias. On the nightside, on average, the wave power is maximum near the equator and decreases with increasing magnetic latitude, suggesting an equatorial source. When the spacecraft traverses the plasma sheet during its equatorial crossings, the wave power is a factor of 2 larger than equatorial crossings that do not cross the plasma sheet. The waves are highly transverse at large magnetic latitudes but are compressional near the equator. However, at the equator the transverse component of these waves increases relative to the compressional component as the degree of polarization decreases. Also, there is a substantial minority of events that are transverse at all magnetic latitudes, including the equator. A few of these latter events could be interpreted as ion cyclotron waves. In general, the waves tend to be strongly linear, have ellipticity magnitudes less than 0.3, and are skewed toward right-handedness, and the wave-normal angles are peaked near 90°. Polarization analysis indicates that a mixture of three wave modes is present, a left-handed (ICW) and a right-handed transverse mode and a compressional mode. For the transverse mode their wave magnetic field variations tend to be oriented perpendicular to the estimated field gradient, a pattern consistent with that of field-line resonances. If these transverse waves are field-line resonances, their standing wave pattern must be composed of at least two traveling waves, and therefore the interpretation of ellipticity and wave-normal angle from polarization analysis is difficult [*Denton et al.*, 1996]. We note that for the transverse wave events plotted in Figure 9c, the events with negative ellipticity have larger power on average than those with positive ellipticity, which matches expectations if the waves are a superposition of two ICW modes. Despite the strong right-handed skew in the polarization analysis, therefore, these waves may be composed mainly of compressional-mode waves and ICWs. Can the compressional and the transverse waves be related? The β_{H+} (Table 2) in this wave environment can be very high, and *Denton et al.* [2010] showed that in Earth's plasma sheet boundary layer the compressional or transverse nature of the electromagnetic ion Bernstein wave mode can be strongly sensitive to β_{H+}. Analysis of loss cone distributions in plasmas of highly variable but high β_{H+} is needed to further delineate the role that these waves play in ion precipitation and in the direct generation of field-line resonances at Mercury.

[37] **Acknowledgments.** The MESSENGER project is supported by the NASA Discovery Program under contracts NAS5–97271 to The Johns Hopkins University Applied Physics Laboratory and NASW-00002 to the Carnegie Institution of Washington. This work is also supported by NASA Planetary Data Analysis Program grant NNX10AU26G.

[38] Masaki Fujimoto thanks the reviewers for their assistance in evaluating the paper.

References

Alexeev, I. I., E. S. Belenkaya, S. Y. Bobrovnikov, J. A. Slavin, and M. Sarantos (2008), Paraboloid model of Mercury's magnetosphere, *J. Geophys. Res.*, *113*, A12210, doi:10.1029/2008JA013368.

Anderson, B. J., R. E. Denton, and S. A. Fuselier (1996), On determining polarization characteristics of ion cyclotron wave magnetic field fluctuations, *J. Geophys. Res.*, *101*, 13,195–13,213, doi:10.1029/96JA00633.

Anderson, B. J., M. H. Acuña, D. A. Lohr, J. Scheifele, A. Raval, H. Korth, and J. A. Slavin (2007), The Magnetometer instrument on MESSENGER, *Space Sci. Rev.*, *131*, 417–450, doi:10.1007/s11214-007-9246-7.

Anderson, B. J., M. H. Acuña, H. Korth, M. E. Purucker, C. L. Johnson, J. A. Slavin, S. C. Solomon, and R. L. McNutt Jr. (2008), The structure of Mercury's magnetic field from MESSENGER's first flyby, *Science*, *321*, 82–85, doi:10.1126/science.1159081.

Anderson, B. J., et al. (2010), The magnetic field of Mercury, *Space Sci. Rev.*, *152*, 307–339, doi:10.1007/s11214-009-9544-3.

Anderson, B. J., C. L. Johnson, H. Korth, M. E. Purucker, R. M. Winslow, J. A. Slavin, S. C. Solomon, R. L. McNutt Jr., J. M. Raines, and T. H. Zurbuchen (2011), The global magnetic field of Mercury from MESSENGER orbital observations, *Science*, *333*, 1859–1862, doi:10.1126/science.1211001.

Arthur, C. W., R. L. McPherron, and J. D. Means (1976), A comparative study of three techniques for using the spectral matrix in wave analysis, *Radio Sci.*, *11*, 833–845, doi:10.1029/RS011i010p00833.

Blomberg, L. G. (1997), Mercury's magnetosphere, exosphere and surface: Low frequency field and wave measurements as a diagnostic tool, *Planet. Space Sci.*, *45*, 143–148, doi:10.1016/S0032-0633(96)00092-X.

Boardsen, S. A., D. L. Gallagher, D. A. Gurnett, W. K. Peterson, and J. L. Green (1992), Funnel-shaped, low-frequency equatorial waves, *J. Geophys. Res.*, *97*, 14,967–14,976, doi:10.1029/92JA00827.

Boardsen, S. A., B. J. Anderson, M. H. Acuña, J. A. Slavin, H. Korth, and S. C. Solomon (2009a), Narrow-band ultra-low-frequency wave observations by MESSENGER during its January 2008 flyby through Mercury's magnetosphere, *Geophys. Res. Lett.*, *36*, L01104, doi:10.1029/2008GL036034.

Boardsen, S. A., J. A. Slavin, B. J. Anderson, H. Korth, and S. C. Solomon (2009b), Comparison of ultra-low-frequency waves at Mercury under northward and southward IMF, *Geophys. Res. Lett.*, *36*, L18106, doi:10.1029/2009GL039525.

Denton, R. E., B. J. Anderson, G. Ho, and D. C. Hamilton (1996), Effects of wave superposition on the polarization of electromagnetic ion cyclotron waves, *J. Geophys. Res.*, *101*, 24,869–24,885, doi:10.1029/96JA02251.

Denton, R. E., M. J. Engebretson, A. Keiling, A. P. Walsh, S. P. Gary, P. M. E. Décréau, C. A. Cattell, and H. Rème (2010), Multiple harmonic ULF waves in the plasma sheet boundary layer: Instability analysis, *J. Geophys. Res.*, *115*, A12224, doi:10.1029/2010JA015928.

Engebretson, M. J., C. R. G. Kahlstorf, J. L. Posch, A. Keiling, A. P. Walsh, R. E. Denton, M. C. Broughton, C. J. Owen, K.-H. Fornaçon, and H. Rème (2010), Multiple harmonic ULF waves in the plasma sheet boundary layer observed by Cluster, *J. Geophys. Res.*, *115*, A12225, doi:10.1029/2010JA015929.

Gary, S. P., K. Liu, D. Winske, and R. E. Denton (2010), Ion Bernstein instability in the terrestrial magnetosphere: Linear dispersion theory, *J. Geophys. Res.*, *115*, A12209, doi:10.1029/2010JA015965.

Glassmeier, K.-H., P. N. Mager, and D. Y. Klimushkin (2003), Concerning ULF pulsations in Mercury's magnetosphere, *Geophys. Res. Lett.*, *30*(18), 1928, doi:10.1029/2003GL017175.

Gurnett, D. A., S. D. Shawhan, N. M. Brice, and R. L. Smith (1965), Ion cyclotron whistlers, *J. Geophys. Res.*, *70*, 1665–1688, doi:10.1029/JZ070i007p01665.

Kim, E.-H., and D.-H. Lee (2003), Resonant absorption of ULF waves near the ion cyclotron frequency: A simulation study, *Geophys. Res. Lett.*, *30*(18), 2240, doi:10.1029/2003GL017918.

Kim, E.-H., J. R. Johnson, and D.-H. Lee (2008), Resonant absorption of ULF waves at Mercury's magnetosphere, *J. Geophys. Res.*, *113*, A11207, doi:10.1029/2008JA013310.

Kim, E.-H., J. R. Johnson, and K.-D. Lee (2011), ULF wave absorption at Mercury, *Geophys. Res. Lett.*, *38*, L16111, doi:10.1029/2011GL048621.

Klimushkin, D. Y., P. N. Mager, and K.-H. Glassmeier (2006), Axisymmetric Alfvén resonances in a multi-component plasma at finite ion gyrofrequency, *Ann. Geophys.*, *24*, 1077–1084, doi:10.5194/angeo-24-1077-2006.

Korth, H., B. J. Anderson, J. M. Raines, J. A. Slavin, T. H. Zurbuchen, C. L. Johnson, M. E. Purucker, R. M. Winslow, S. C. Solomon, and R. L. McNutt Jr. (2011), Plasma pressure in Mercury's equatorial magnetosphere derived from MESSENGER Magnetometer observations, *Geophys. Res. Lett.*, *38*, L22201, doi:10.1029/2011GL049451.

Lee, D.-H., J. R. Johnson, K. Kim, and K.-S. Kim (2008), Effects of heavy ions on ULF wave resonances near the equatorial region, *J. Geophys. Res.*, *113*, A11212, doi:10.1029/2008JA013088.

McIlwain, C. E. (1972), Plasma convection in the vicinity of the geosynchronous orbit, in *Earth Magnetospheric Processes*, edited by B. M. McCormac, pp. 268–279, D. Reidel, Hingham, Mass., doi:10.1007/978-94-010-2896-7_27.

Means, J. D. (1972), Use of the three-dimensional covariance matrix in analyzing the polarization properties of plane waves, *J. Geophys. Res.*, *77*, 5551–5559, doi:10.1029/JA077i028p05551.

Othmer, C., K. H. Glassmeier, and R. Cramm (1999), Concerning field line resonances in Mercury's magnetosphere, *J. Geophys. Res.*, *104*, 10,369–10,378, doi:10.1029/1999JA900009.

Raines, J. M., J. A. Slavin, T. H. Zurbuchen, G. Gloeckler, B. J. Anderson, D. N. Baker, S. M. Krimigis, H. Korth, and R. L. McNutt Jr. (2011), MESSENGER observations of the plasma environment near Mercury, *Planet. Space Sci.*, *59*, 2004–2015, doi:10.1016/j.pss.2011.02.004.

Rauch, J. L., and A. Roux (1982), Ray tracing of ULF waves in a multicomponent magnetospheric plasma: Consequences for the generation mechanism of ion cyclotron waves, *J. Geophys. Res.*, *87*, 8191–8198, doi:10.1029/JA087iA10p08191.

Russell, C. T. (1989), ULF waves in the Mercury magnetosphere, *Geophys. Res. Lett.*, *16*, 1253–1256, doi:10.1029/GL016i011p01253.

Schriver, D., et al. (2011), Quasi-trapped particle population around Mercury, *Geophys. Res. Lett.*, *38*, L23103, doi:10.1029/2011GL049629.

Slavin, J. A., et al. (2008), Mercury's magnetosphere after MESSENGER's first flyby, *Science*, *321*, 85–89, doi:10.1126/science.1159040.

Slavin, J. A., et al. (2009), MESSENGER observations of magnetic reconnection in Mercury's magnetosphere, *Science*, *324*, 606–610, doi:10.1126/science.1172011.

Southwood, D. J. (1997), The magnetic field of Mercury, *Planet. Space Sci.*, *45*, 113–117, doi:10.1016/S0032-0633(96)00105-5.

Stix, T. H. (1992), *Waves in Plasmas*, 566 pp., Am. Inst. of Phys., Springer, New York.

Trávníček, P. M., D. Schriver, P. Hellinger, D. Herčík, B. J. Anderson, M. Sarantos, and J. A. Slavin (2010), Mercury's magnetosphere-solar wind interaction for northward and southward interplanetary magnetic field: Hybrid simulation results, *Icarus*, *209*, 11–22, doi:10.1016/j.icarus.2010.01.008.

Zhu, X., and M. G. Kivelson (1989), Global mode ULF pulsations in a magnetosphere with a nonmonochromatic Alfvén velocity profile, *J. Geophys. Res.*, *94*, 1479–1485, doi:10.1029/JA094iA02p01479.

Zurbuchen, T. H., J. M. Raines, G. Gloeckler, S. M. Krimigis, J. A. Slavin, P. L. Koehn, R. M. Killen, A. L. Sprague, R. L. McNutt Jr., and S. C. Solomon (2008), MESSENGER observations of the composition of Mercury's ionized exosphere and plasma environment, *Science*, *321*, 90–92, doi:10.1126/science.1159314.

Zurbuchen, T. H., et al. (2011), MESSENGER observations of the spatial distribution of planetary ions near Mercury, *Science*, *333*, 1862–1865, doi:10.1126/science.1211302.